

# Defect chemistry and proton-dopant association in BaZrO<sub>3</sub> and BaPrO<sub>3</sub>†

Stephen J. Stokes and M. Saiful Islam\*

Received 5th February 2010, Accepted 24th May 2010

DOI: 10.1039/c0jm00328j

Defect reactions, water incorporation and proton-dopant association in the BaZrO<sub>3</sub> and BaPrO<sub>3</sub> perovskite materials are investigated using well-established atomistic simulation techniques. The interatomic potential models reproduce the experimental cubic BaZrO<sub>3</sub> and orthorhombic BaPrO<sub>3</sub> structures. The high defect energies suggest that significant intrinsic disorder (either Frenkel, Schottky or reduction) in BaZrO<sub>3</sub> is unlikely, which is consistent with the relative chemical stability of this system. In contrast, favourable redox processes are found for intrinsic reduction of BaPrO<sub>3</sub>, and oxidation of acceptor-doped BaPrO<sub>3</sub>, the latter leading to p-type conduction properties as observed experimentally. Binding energies for dopant-OH pairs in BaZrO<sub>3</sub> indicate the weakest association for Gd and Y dopants, and the strongest association for Sc. The high binding energies for all the dopant-OH pair clusters in BaPrO<sub>3</sub> suggest strong proton trapping effects, which would be detrimental to proton conductivity. The water incorporation or hydration energy is found to be less exothermic for BaZrO<sub>3</sub> than for BaPrO<sub>3</sub>, the higher exothermic value for the latter suggesting that water incorporation extends to higher temperatures in accord with the available thermodynamic data. The energies and pathways for oxide ion migration in both materials are also investigated.

## 1 Introduction

Solid-state proton conductors based on cerate and zirconate perovskite oxides have attracted considerable attention for a range of electrochemical applications, such as fuel cells, separation membranes and steam electrolyzers.<sup>1–7</sup> Such oxide materials are particularly attractive as electrolytes for solid oxide fuel cells (SOFCs) operating at intermediate temperatures (400–700 °C), in contrast to high temperature operation (> 900 °C) of SOFCs based on the Y/ZrO<sub>2</sub> oxide-ion conductor.

Of the known perovskite-type proton conductors, there has been considerable experimental<sup>8–30</sup> and computational<sup>31–39</sup> interest in acceptor-doped BaZrO<sub>3</sub> due to its high proton conductivity in a cubic structure coupled with good chemical and mechanical stability. The proton mobility in Y-doped BaZrO<sub>3</sub> is among one of the highest ever reported for a perovskite-type proton conductor, and has the potential to operate at lower temperatures than the conventional SOFC electrolyte. There has also been recent interest in some less-studied Ba-based perovskites as potential proton conductors including acceptor-doped BaPrO<sub>3</sub>,<sup>40–48</sup> but the thermodynamic and conduction properties of these materials are not fully characterised.

It is known that defect reactions and atomistic diffusion mechanisms underpins the fundamental understanding of proton conduction behaviour. However, there is often limited atomic-scale information on complex ceramic oxides, such as lattice

defects, local proton sites and the extent of interactions between the dopant ion and the protonic defect leading to possible proton trapping. Yamazaki *et al.*<sup>23</sup> have reported thermogravimetry studies of the water incorporation reaction in Y-doped BaZrO<sub>3</sub> and determined hydration enthalpies that are substantially smaller than those reported previously.<sup>8</sup> In support of previous computer modelling predictions<sup>39,39</sup> recent Neutron-Spin-Echo experiments<sup>14</sup> on hydrated BaZr<sub>0.90</sub>Y<sub>0.10</sub>O<sub>2.95</sub> report data that are indicative of trapping effects in which the proton spends an extended time in the vicinity of the Y dopant before further proton diffusion.

This study attempts to provide further insight into these issues by using atomistic simulation techniques, which have been applied successfully in studies of ionic conduction in a range of complex oxides including CaZrO<sub>3</sub>,<sup>49,50</sup> ACeO<sub>3</sub>,<sup>51–53</sup> and LaBaGaO<sub>4</sub>.<sup>54,55</sup> This paper presents recent computational studies of topical proton-conducting perovskites based upon BaZrO<sub>3</sub> and BaPrO<sub>3</sub>, with an examination of trends and direct comparison with experimental data where available. Emphasis here is placed on probing the defect chemistry, proton sites, dopant-OH association and oxygen ion migration on the atomic-scale.

## 2 Simulation methods

Detailed reviews of these well established techniques are given elsewhere,<sup>56</sup> so only a brief account will be presented here. The calculations are within the framework of the Born model of ionic solids, with ion-ion interactions treated by long-range Coulombic terms and short-range forces that account for electron cloud overlap (Pauli repulsion) and dispersion (Van der Waals) interactions. The short-range interactions are modelled with a Buckingham interatomic potential:

Department of Chemistry, University of Bath, Bath, BA2 7AY, UK.  
E-mail: M.S.Islam@bath.ac.uk

† This paper is part of a *Journal of Materials Chemistry* themed issue on proton transport for fuel cells. Guest editors: Sossina Haile and Peter Pintauro.

**Table 1** Interatomic potentials and shell model parameters for BaZrO<sub>3</sub> and BaPrO<sub>3</sub>

<b>(i) short-range</b>			
Interaction	<i>A</i> (eV)	$\rho$ (Å)	<i>C</i> (eV Å <sup>6</sup> )
Ba <sup>2+</sup> ...O <sup>2-</sup>	931.700	0.3949	0.000
Zr <sup>4+</sup> ...O <sup>2-</sup>	985.869	0.3760	0.000
Pr <sup>4+</sup> ...O <sup>2-</sup>	1925.382	0.3511	21.152
O <sup>2-</sup> ...O <sup>2-</sup>	22764.300	0.1490	27.890
<b>(ii) shell model</b>			
Species	<i>Y</i> ( <i>e</i> )	<i>k</i> (eV Å <sup>-2</sup> )	
Ba <sup>2+</sup>	1.460	14.800	
Zr <sup>4+</sup>	1.350	169.617	
Pr <sup>4+</sup>	7.7	291	
O <sup>2-</sup>	-2.077	27.300	

**Table 2** Parameters for O–H interaction

Morse potential	<i>D</i> (eV)	$\beta$ (Å <sup>-1</sup> )	<i>r</i> <sub>0</sub> (Å)
O...H	7.0525	2.1986	0.9485
Buckingham potential	<i>A</i> (eV)	$\rho$ (Å)	<i>C</i> (eV Å <sup>6</sup> )
O...H	311.97	0.25	0

$$V_{ij}(r) = A \exp^{-r/\rho_{ij}} - \frac{C_{ij}}{r^6} \quad (1)$$

where  $A_{ij}$ ,  $r_{ij}$  and  $C_{ij}$  are empirically derived parameters for each ion-ion interaction. Polarizability of the ions is incorporated by using the Dick–Overhauser shell model.<sup>57</sup> The lattice energy calculations employ the now standard Ewald summation procedures for the Coulombic interactions.

An important feature of the calculations is the treatment of lattice relaxation about the point defect or dopant. The Mott–Littleton approach<sup>58</sup> used here involves the partitioning of the crystal lattice into two regions so that over 500 ions within the spherical inner region surrounding the defect are relaxed explicitly. The remainder of the crystal, where the defect forces are relatively weak, are treated by more approximate quasi-continuum methods. In this way, local relaxation about the defect or impurity was effectively modelled and the crystal was not considered simply as a rigid lattice. These methods are embodied in the GULP simulation code.<sup>59</sup>

The interatomic potential and shell model parameters for BaZrO<sub>3</sub> and BaPrO<sub>3</sub> are listed in Table 1. The parameters for Ba–O, Zr–O and O–O have been transferred from previous simulation studies,<sup>60,61</sup> and those for Pr–O have been derived empirically for this study. For the protonic defect, the O–H interaction was modelled using an attractive Morse potential

$$V(r) = D\{1 - \exp[-\beta(r - r_0)]\}^2 \quad (2)$$

using parameters (Table 2) developed from ab initio quantum mechanical cluster calculations, with a point charge representation of the surrounding lattice.<sup>62</sup> The dipole of the hydroxyl species was distributed across both ions to give an overall charge of -1 with O assigned -1.4263 and H +0.4263. An additional Buckingham potential describing the interaction between the hydroxyl group and the lattice ions was taken from previous studies of water incorporation in silicates.<sup>63</sup> This simulation approach has been applied successfully to other proton-conducting perovskites,<sup>49,50,52,64</sup> and more recently, to water incorporation in Si/Ge-apatites.<sup>65</sup>

## 3 Results and discussion

### 3.1 Structural modelling and defect formation

The starting point of the study, before carrying out defect calculations, was to reproduce the experimentally observed crystal structures. The unit cell dimensions and ion positions were equilibrated under constant pressure conditions. The calculated structures of cubic BaZrO<sub>3</sub> and orthorhombic BaPrO<sub>3</sub> are compared with experiment in Table 3. The unit cell parameters change only slightly on relaxation of the structures. The differences in the observed and calculated lattice parameters and bond lengths are all within 0.09 Å, and in many cases less than 0.03 Å, indicating that the potentials reproduce these perovskite structures.

Energies of isolated point defects (vacancies and interstitials) were then calculated for BaZrO<sub>3</sub> and BaPrO<sub>3</sub>. The isolated defect energies were combined to give the energies of formation of Frenkel and Schottky defects based on the following eqn (3)–(8); note that Kroger–Vink notation is used where, for example, O<sub>O</sub><sup>x</sup>, V<sub>O</sub><sup>\*\*</sup> and O<sub>i</sub><sup>'</sup>, indicates a lattice anion, an oxygen vacancy (+2 effective charge) and an oxygen interstitial (-2 effective charge) respectively.

Ba Frenkel:



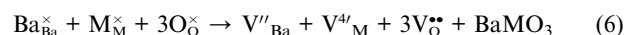
M Frenkel:



O Frenkel:



Schottky:



BaO Schottky-type:

**Table 3** Experimental and calculated lattice parameters and mean bond lengths for BaZrO<sub>3</sub> and BaPrO<sub>3</sub>

Parameter	Exp	Calc	$\delta$
<b>BaZrO<sub>3</sub><sup>a</sup></b>			
<i>a</i> = <i>b</i> = <i>c</i> /Å	4.199	4.188	-0.011
Ba–O/Å	2.969	2.961	-0.008
Zr–O/Å	2.099	2.094	-0.005
<b>BaPrO<sub>3</sub><sup>b</sup></b>			
<i>a</i> /Å	6.181	6.213	-0.032
<i>b</i> /Å	6.214	6.221	-0.007
<i>c</i> /Å	8.722	8.789	-0.067
Ba–O1/Å	3.114	3.111	-0.003
Ba–O2/Å	3.016	3.110	0.093
Pr–O1/Å	2.227	2.205	0.022
Pr–O2/Å	2.223	2.203	0.020

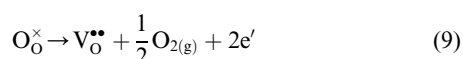
<sup>a</sup> Ref. 66. <sup>b</sup> Ref. 67.

MO<sub>2</sub> Schottky-type:

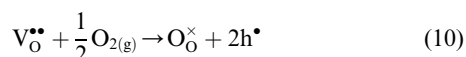


The resulting energies are listed in Table 4 which reveal two main points. First, the creation of Frenkel defects is associated with substantial amounts of energy, confirming that the close-packed perovskite structure is highly unlikely to accommodate ion interstitials. Second, the most favourable energy is found for the BaO Schottky-type disorder for both systems, with the lowest value of 2.13 eV for BaPrO<sub>3</sub>. This suggests the possible loss of BaO at very high temperatures. It has been found that BaPrO<sub>3</sub>-based compounds seem to exhibit greater chemical instability.

Most applications of proton conductors require them to be used under a range of redox (reducing or oxidising) conditions. For the undoped system, the following reaction for reduction can be considered involving the creation of oxygen vacancies and electronic defects:



For an extrinsic system, where oxygen vacancies already exist due to acceptor doping, oxidation can occur *via* the following reaction:



in which the oxygen vacancies are filled to create electron holes ( $h^{\bullet}$ ). Our approach to electronic defects in BaZrO<sub>3</sub> and BaPrO<sub>3</sub> follows that used for the BaCeO<sub>3</sub> and SrCeO<sub>3</sub> perovskites,<sup>52,64</sup> in which the hole/electronic species are treated as small polarons localised at ion sites: hence, hole centres are modelled as an O<sup>-</sup> substituted at O<sup>2-</sup> and the electron centres ( $e'$ ) as a M<sup>3+</sup> substituted at M<sup>4+</sup>. The corresponding interatomic potentials are transferred directly for the short-range Buckingham parameters, but the shell model is modified by changing the shell charge by one. Using these electronic terms, the energies of the redox reactions were calculated and are given in Table 5. Owing to the uncertainties in the free-ion terms employed, we must be cautious in giving detailed interpretations, although these methods have been shown to provide reliable trends in overall redox energies.

**Table 4** Energies of Frenkel and Schottky disorder in BaZrO<sub>3</sub> and BaPrO<sub>3</sub> (eV/defect)

Type	BaZrO <sub>3</sub>	BaPrO <sub>3</sub>
Ba Frenkel	6.97	5.96
M Frenkel	10.22	12.78
O Frenkel	5.58	4.89
Schottky	3.20	4.49
BaO Schottky-type	2.80	2.13
MO <sub>2</sub> Schottky-type	3.75	5.30

**Table 5** Energies of redox reactions in BaZrO<sub>3</sub> and BaPrO<sub>3</sub> (eV/electronic defect)

Type	BaZrO <sub>3</sub>	BaPrO <sub>3</sub>
Oxidation	2.90	2.15
Reduction	6.23	1.14

The results show that the lowest oxidation and reduction energies are found for the BaPrO<sub>3</sub> system, suggesting a greater concentration of electronic defects in this material. For the doped material, p-type conductivity will be exhibited with increasing oxygen partial pressures. Indeed, Furøy *et al.*<sup>40</sup> show that Gd-doped BaPrO<sub>3</sub> is dominated by electronic holes at lower temperatures in oxidising atmospheres, making it a p-type conductor. Similarly, Magraso *et al.*<sup>47</sup> find that Gd-doped BaPrO<sub>3</sub> is largely a p-type conductor.

The lowest defect reaction energy is for intrinsic reduction of BaPrO<sub>3</sub> with the formation of oxygen vacancies and electronic species (Pr<sup>3+</sup>). Furøy *et al.*<sup>40</sup> find that the BaPrO<sub>3</sub> system is unstable towards reduction, while photoemission spectroscopy measurements of Mimuro *et al.*<sup>46</sup> indicate the presence of Pr<sup>3+</sup> in the intrinsic region.

The high reduction energy in BaZrO<sub>3</sub> indicates greater resistance to reduction than oxidation, as observed experimentally.<sup>24</sup> We note that entropic effects need to be included in our calculations to derive a quantitative relationship between oxygen partial pressure and defect concentration, which is a topic for further study. In general, these results are consistent with experimental findings of the two materials, which show mixed ionic/electronic conductivity and that p-type electronic conductivity increases with increasing oxygen activity especially for doped BaPrO<sub>3</sub>.

### 3.2 Water incorporation and protonic defect

Acceptor doping with trivalent cations (typically Y, Yb or In) onto the Zr<sup>4+</sup> or Pr<sup>4+</sup> site generates oxygen vacancies as charge-compensating defects. The incorporation of water into the perovskite structure is achieved by treatment in water vapour, in which the oxygen vacancies are replaced by protonic defects (in the form of hydroxyl ions) as shown by the following equation,



Previous QM computational studies<sup>8,31,32,36,68,69</sup> have indicated that proton conduction in perovskites involves (i) proton hopping between neighbouring oxygens (Grotthuss mechanism) aided by local lattice softening and (ii) low activation barrier rotational motion of the hydroxyl group and rate-limiting proton transfer toward a neighbouring oxide ion. These studies also suggest possible quantum effects (tunnelling) for the proton jump. Hence, the characterisation of the local structure and O–H configurations is important.

As with previous studies,<sup>49,52</sup> our simulation techniques can be used to probe the proton site and examine the most energetically favourable O–H configuration. The simulations indicate that the equilibrium O–H bond lies perpendicular to the line between the two adjacent Zr<sup>4+</sup> or Pr<sup>4+</sup> ions (as shown in Fig. 1 for BaZrO<sub>3</sub>). This configuration seems to maximise both the H–Ba<sup>2+</sup> and the H–M<sup>4+</sup> distances.

Unlike average structural techniques, our atomistic simulations reveal local ion relaxations around the protonic defect (illustrated in Fig. 1b) with a local distortion from cubic symmetry for BaZrO<sub>3</sub>. An equilibrium O–H distance of 0.98 Å is found, which lies close to accepted O–H bond lengths in perovskites.<sup>3,4</sup> Our calculated position for the H atom in BaZrO<sub>3</sub> is

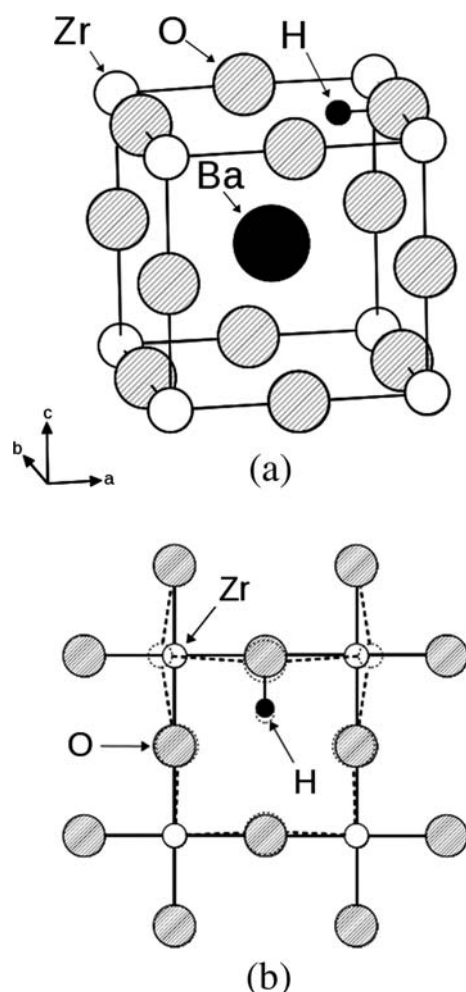


**Fig. 1** Schematic of equilibrium O–H configuration in BaZrO<sub>3</sub> (a) Unit cell of cubic structure (b) relaxed (dotted line) and unrelaxed local structure in the a–b plane.

(0.5, 0.275, 0.0). These results accord well with the deuteron position refined from neutron powder diffraction data collected on deuterated and dry samples of BaZr<sub>0.5</sub>In<sub>0.5</sub>O<sub>2.75</sub> at 5 K and room temperature.<sup>11</sup>

Based on reaction (11), the energy of water incorporation, or hydration energy, ( $E_{\text{H}_2\text{O}}$ ) can be calculated by using the following equation:

$$E_{\text{H}_2\text{O}} = 2E_{\text{OH}} - E_{\text{VO}^{\bullet\bullet}} + E_{\text{PT}} \quad (12)$$

where  $E_{\text{OH}}$  is the energy associated with substitution of O<sup>2-</sup> with an OH<sup>-</sup> group,  $E_{\text{VO}^{\bullet\bullet}}$  is the oxygen vacancy energy, and  $E_{\text{PT}}$  is

**Table 6** Defect and hydration energies in BaZrO<sub>3</sub> and BaPrO<sub>3</sub>

	BaZrO <sub>3</sub>	BaPrO <sub>3</sub>
$E_{\text{VO}^{\bullet\bullet}}/\text{eV}$	18.56	19.01
$E_{\text{OH}}/\text{eV}$	15.11	14.67
Calc. $E_{\text{H}_2\text{O}}/\text{eV}$	-0.12	-1.45
Exp. $E_{\text{H}_2\text{O}}/\text{eV}$	-0.22 to -0.27 <sup>a</sup> , -0.82 to -0.97 <sup>b</sup>	—

<sup>a</sup> Ref. 23. <sup>b</sup> Ref. 8.

the energy of the gas phase reaction  $\text{O}^{2-} + \text{H}_2\text{O} = 2\text{OH}^-$ . The latter term is estimated from the difference between proton affinities of O<sup>2-</sup> and OH<sup>-</sup>, and discussed in detail by Catlow and co-workers.<sup>70,71</sup>

The calculated hydration energies are listed in Table 6 and reveal two key features. First,  $E_{\text{H}_2\text{O}}$  is negative for both BaZrO<sub>3</sub> and BaPrO<sub>3</sub>, which indicates that the materials will be dominated by protons at low temperatures and oxygen vacancies at high temperatures. Second, the magnitude of  $E_{\text{H}_2\text{O}}$  is notably less exothermic for BaZrO<sub>3</sub> than that for BaPrO<sub>3</sub>. Yamazaki *et al.*<sup>23</sup> determine hydration enthalpies at low temperature for Y doped BaZrO<sub>3</sub> of -22 to -26 kJmol<sup>-1</sup> (-0.22 to -0.27 eV) with varying dopant levels of 20–40%. As with our calculated value, these are significantly smaller in magnitude than the previously reported values for Y-doped BaZrO<sub>3</sub> of -79.4 to -93.3 kJmol<sup>-1</sup> (-0.82 to -0.97 eV).<sup>8</sup> Yamazaki *et al.*<sup>23</sup> indicate that the smaller negative values in comparison with previous data are attributed to the restriction of the analysis to the low temperatures at which electronic hole concentrations can be neglected.

For BaPrO<sub>3</sub>, there is no experimental hydration enthalpy for direct comparison partly due to the dominance of electronic behaviour. Mimuro *et al.*<sup>46</sup> indicate that the proton solubility increases with increasing dopant concentration in Yb-doped BaPrO<sub>3</sub>, while Magraso *et al.*<sup>47</sup> find Gd-doped BaPrO<sub>3</sub> to be highly reactive under water, CO<sub>2</sub> and hydrogen containing atmospheres.

### 3.3 Proton-dopant interactions

There has been some debate as to whether there is any significant association between the dopant ion and the protonic defect (hydroxyl ion at oxygen site), which may affect proton mobility. In an attempt to probe the question of proton-dopant association, we have extended our previous studies on SrCeO<sub>3</sub><sup>52</sup> and CaZrO<sub>3</sub><sup>69</sup> with a series of calculations on OH-dopant pairs in BaZrO<sub>3</sub> and BaPrO<sub>3</sub> comprised of a hydroxyl ion and a neighbouring dopant substitutional (Fig. 2). With regard to the relaxed geometry, deviations from the equilibrium O–H configuration (shown in Fig. 1) are found, corresponding to a shift of

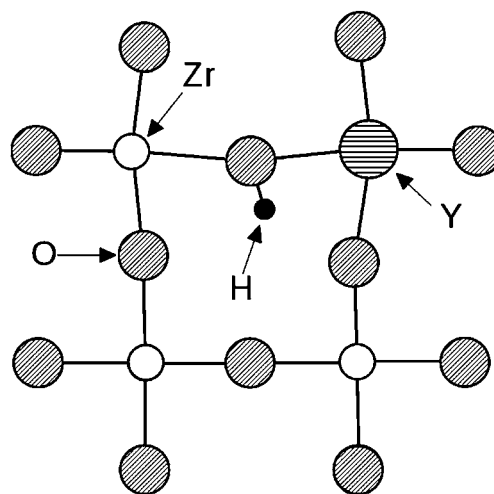


**Fig. 2** Calculated local structure for the OH<sub>O'</sub>-Y<sub>Zr'</sub> pair cluster in BaZrO<sub>3</sub> showing local lattice relaxation.

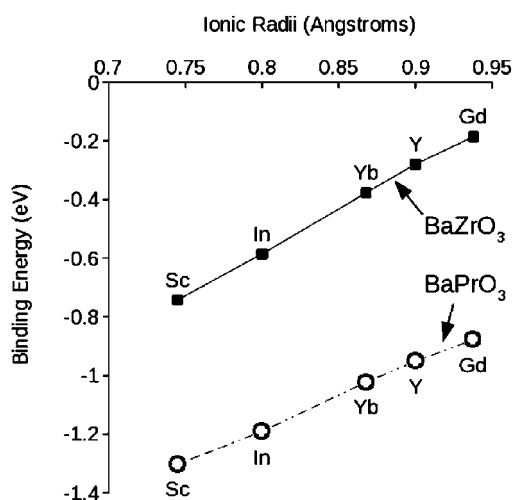


Fig. 3 Dopant-OH binding energies as a function of dopant ion size.

the H position towards a neighbouring oxygen and dopant ion (shown in Fig. 2 for  $Y^{3+}$  in  $BaZrO_3$  as an example). As in Fig. 1b, the simulations reveal ion relaxations and local deviations from cubic symmetry in  $BaZrO_3$ .

The cluster binding energy ( $E_{\text{bind}}$ ) for this configuration was calculated, which is defined as the difference between the energy of the cluster ( $E_{\text{cluster}}$ ) and the sum of the energies of the corresponding isolated defects; this is given by the general relation:

$$E_{\text{bind}} = E_{\text{cluster}} - \left( \sum_{\text{component}} E_{\text{isolated defect}} \right) \quad (13)$$

where a negative value indicates that the cluster is stable with respect to the component isolated defects. For example, in the case of  $BaZrO_3$  the binding energy is given by the relation:

$$E_{\text{bind}} = E(\text{OH}_O \cdot \text{M}_{\text{Zr}'}) - \{E(\text{M}_{\text{Zr}'}) + E(\text{OH}_O)\} \quad (14)$$

Attention was focused on commonly used dopants in these materials, namely Sc, In, Y, Yb and Gd. The resulting energies (reported in Fig. 3) predict that all the hydroxyl-dopant pairs are favourable configurations. The lowest binding energy are for Y and Gd, and the strongest association is for Sc. These results

Table 7 Dopant-proton (M–H) distances in the pair cluster (Fig. 2) in  $BaZrO_3$  and  $BaPrO_3$

System	$M^{3+}$	ionic radius (Å)	M–H (Å)	$\Delta M\text{--}H(\text{Å})$
$BaZrO_3$	Zr	0.72	2.65	0.00
	Sc	0.75	2.25	–0.40
	In	0.80	2.29	–0.36
	Yb	0.87	2.36	–0.29
	Y	0.90	2.41	–0.24
	Gd	0.94	2.81	0.16
$BaPrO_3$	Pr	0.85	2.82	0.00
	Sc	0.75	2.24	–0.58
	In	0.80	2.27	–0.55
	Yb	0.87	2.31	–0.51
	Y	0.90	2.34	–0.48
	Gd	0.94	2.37	–0.45

indicate that proton mobility would be very sensitive to the type of acceptor dopant ion, and may be related to basicity as well ion size factors. It may be significant that a low binding energy is found for  $Y^{3+}$ , which is the most commonly used dopant in the  $BaZrO_3$  proton conductor. It should be noted there is limited research relating to Gd-doped  $BaZrO_3$  and hence our results show that Gd doping warrants further investigation.

Kreuer *et al.*<sup>8</sup> have investigated a range of alkaline-earth zirconates and titanates for potential electrochemical applications; they find that the system  $BaZr_{1-x}Y_xO_{3-\delta}$  ( $x = 0.1$ ) exhibits the highest proton mobility and the lowest activation enthalpy. In contrast, the lowest proton mobility and highest activation energy is found for Sc-doped  $BaZrO_3$ , for which we predict the strongest dopant-OH association. Our binding energy results for  $BaPrO_3$  indicate extremely strong proton trapping by all of the acceptor dopants. This indicates significant impeding effects on long-range proton mobility, which would lead to low proton conductivity in doped  $BaPrO_3$ .

The interatomic distances between the M dopant and proton of the hydroxyl unit in the dopant-OH cluster have been analysed and are listed in Table 7. The analysis reveals that the distance between M and the proton (M–H) change with respect to the host Zr and Pr ions. The longest M–H distance are for the Gd and Y dopants, and mirrors the variation in binding energy (Fig. 3). Interestingly, the largest dopant (Gd) in  $BaZrO_3$  is the only case in which the O–H bond does not swing towards the dopant ion, which can be related to the greater ion size mismatch between the  $Zr^{4+}$  and  $Gd^{3+}$  cations.

Although there are no quantitative experimental values for either  $BaZrO_3$  or  $BaPrO_3$  for direct comparison, our calculated binding energies agree well with proton “trapping” energies of about –0.2 and –0.4 eV for related Sc-doped  $SrZrO_3$  and Yb-doped  $SrCeO_3$  respectively, derived from muon spin relaxation ( $\mu\text{SR}$ ) and quasi-elastic neutron scattering (QENS) experiments.<sup>72,73</sup> In accord with our previous simulations on dopant-OH interactions in  $SrZrO_3$ ,  $CaZrO_3$ <sup>49,69</sup> and  $SrCeO_3$ ,<sup>52</sup> Bjorketun *et al.*<sup>35</sup> also find proton-dopant cluster formation in  $BaZrO_3$  from DFT-based calculations with association energies of about 0.2–0.4 eV. Moreover, recent Neutron-Spin-Echo (NSE) experiments<sup>14</sup> on proton dynamics in hydrated  $BaZr_{0.90}Y_{0.10}O_{2.95}$  indicate proton trapping in which the proton spends an extended times in the vicinity of the Y dopant ions before further diffusion.

### 3.4 Oxide-ion migration

The oxygen vacancies required for incorporation of protons may also migrate, particularly at high temperature ( $> 600$  °C) when the exothermic incorporation of water is no longer favoured (eqn (11)). Whereas oxygen transport may be disadvantageous for certain applications, steam permeation (involving simultaneous diffusion of protons and oxygen vacancies) has been shown to inhibit coking of the anode in a proton conducting fuel cell operating on methane.<sup>74</sup> In this context, atomistic simulation of oxygen migration may greatly assist in our understanding of the energies and mechanistic features of oxygen transport in these  $BA\text{MO}_3$  systems. Our simulation methods have previously been used to elucidate oxygen-ion migration pathways in many perovskite oxides.<sup>52,53,55</sup>

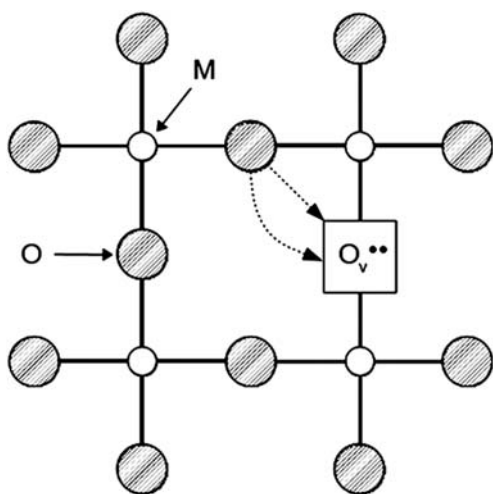
**Table 8** Oxygen vacancy migration energies for BaZrO<sub>3</sub> and BaPrO<sub>3</sub>

Compound	Calc $E_{mig}$ (eV)	Exp $E_{mig}$ (eV)
BaZrO <sub>3</sub>	0.65	0.71 <sup>a</sup>
BaPrO <sub>3</sub>	0.93	—

<sup>a</sup> Ref. 13.

The energy profile of a migrating oxide ion was calculated by placing the ion at intermediate sites between adjacent oxygen vacancies along edges of a MO<sub>6</sub> octahedron. The migration energy ( $E_{mig}$ ) for these pathways (listed in Table 8) show that BaPrO<sub>3</sub> has the highest value. It is important to note that these calculated migration energies ( $E_{mig}$ ) relates to the intrinsic migration (or jump) of an oxygen vacancy, and does not include energies of defect formation or association. As with fluorite-oxides, the bulk activation energy for oxygen ion conduction in perovskites will usually consist of the migration term ( $E_m$ ) at high temperatures, but an additional binding term ( $E_{bind}$ ) at low temperatures, leading to two slopes in the conductivity data. Hence, we recognise that direct comparison between our calculated migration energies and the experimental activation energies ( $E_a$ ) is not straightforward. Also, the  $E_a$  values from experimental studies can show significant variation, which may reflect differences in synthesis conditions, phase purity or analysis of the conductivity data. Nevertheless, the calculated migration energy (0.65eV) for BaZrO<sub>3</sub> is consistent with the experimental activation energies (~0.7eV) for doped BaZrO<sub>3</sub> for high temperatures.<sup>13</sup>

It was found that for BaPrO<sub>3</sub> the migration pathway was not a linear pathway, but curved away from the M site cation, with a deviation from linear of about 0.3Å (Fig. 4). This is a common trait among perovskites which was first predicted for Sr/Mg doped LaGaO<sub>3</sub> using similar computational methods<sup>53</sup> and then observed experimentally using neutron diffraction and the maximum entropy method (MEM).<sup>75</sup> Unusually, BaZrO<sub>3</sub> was found to have a linear oxygen vacancy migration pathway, which would be interesting to examine using a similar neutron diffraction MEM analysis employed by Yashima *et al.*<sup>75,76</sup>

**Fig. 4** Schematic representation of the linear and curved paths of oxygen migration in the ab plane of the BaMO<sub>3</sub> perovskite.

## 4 Conclusions

This study has provided atomic-scale insights into defect reactions and proton-dopant association in BaZrO<sub>3</sub> and BaPrO<sub>3</sub> materials, which are relevant to their proton transport properties for potential intermediate temperature SOFC applications. The main points are summarised as follows:

(1) The high defect energies indicate that significant intrinsic disorder (either Frenkel, Schottky or reduction) in BaZrO<sub>3</sub> is unlikely, which is consistent with the relative chemical stability of this system. In contrast, favourable redox energies are found for intrinsic reduction of BaPrO<sub>3</sub> (creating Pr<sup>3+</sup> species), and oxidation of acceptor-doped BaPrO<sub>3</sub> (creating electronic holes). The latter result predicts p-type conductivity in doped BaPrO<sub>3</sub> in oxidising atmospheres, as observed experimentally.

(2) Binding energies for dopant-OH pairs in BaZrO<sub>3</sub> indicate the weakest association for Gd and Y dopants, and the strongest association for Sc. These results confirm that local proton trapping and mobility would be very sensitive to the type of acceptor dopant ion. The Gd-doped BaZrO<sub>3</sub> system may require further experimental investigation. Our results are compatible with recent Neutron-Spin-Echo measurements of hydrated Y-doped BaZrO<sub>3</sub>, which report data that are indicative of proton trapping. For BaPrO<sub>3</sub> the high binding energies for all the dopant-OH pair clusters indicate strong proton trapping effects, which would be detrimental to proton conductivity.

(3) The water incorporation or hydration energy is found to be less exothermic for BaZrO<sub>3</sub> than for BaPrO<sub>3</sub>, the higher exothermic value for the latter suggesting that water incorporation extends to higher temperatures, in accord with the available thermodynamic analysis. The simulations show significant local lattice relaxation around the OH defect and the OH-dopant clusters, with short-range distortions away from the average cubic symmetry of BaZrO<sub>3</sub>, which will influence proton transport.

(4) Oxide ion migration is predicted to follow a curved path for BaPrO<sub>3</sub> (as observed for the LaGaO<sub>3</sub>-based oxide-ion conductor), but a linear path for the BaZrO<sub>3</sub> system. This warrants further study by, for example, neutron diffraction and maximum entropy methods.

## References

- H. Iwahara, *Solid State Ionics*, 1992, **53-6**, 575.
- H. Iwahara, T. Esaka, H. Uchida and N. Maeda, *Solid State Ionics*, 1981, **3-4**, 359.
- K. D. Kreuer, *Annu. Rev. Mater. Res.*, 2003, **33**, 333.
- K. D. Kreuer, S. J. Paddison, E. Spohr and M. Schuster, *Chem. Rev.*, 2004, **104**, 4637.
- T. Norby, M. Wideroe, R. Glockner and Y. Larring, *Dalton Trans.*, 2004, **19**, 3012.
- L. Malavasi, C. A. J. Fisher and M. S. Islam, *Chem. Soc. Rev.*, 2010, DOI: 10.1039/b915141a.
- S. M. Haile, *Acta Mater.*, 2003, **51**, 5981.
- K. D. Kreuer, S. Adams, W. Munch, A. Fuchs, U. Klock and J. Maier, *Solid State Ionics*, 2001, **145**, 295.
- S. M. Haile, G. Staneff and K. H. Ryu, *J. Mater. Sci.*, 2001, **36**, 1149.
- H. G. Bohn and T. Schober, *J. Am. Cer. Soc.*, 2000, **83**, 768.
- I. Ahmed, C. S. Knee, M. Karlsson, S.-G. Eriksson, P. F. Henry, A. Matic, D. Engberg and L. Borjesson, *J. Alloys Compd.*, 2008, **450**, 103.
- I. Ahmed, M. Karlsson, S.-G. Eriksson, E. Ahlberg, C. S. Knee, K. Larsson, A. K. Azad, A. Matic and L. Borjesson, *J. Am. Ceram. Soc.*, 2008, **91**, 3039.

- 13 I. Ahmed, S.-G. Eriksson, E. Ahlberg, C. S. Knee, H. Gotlind, L.-G. Johansson, M. Karlsson, A. Matic and L. Borjesson, *Solid State Ionics*, 2007, **178**, 515.
- 14 M. Karlsson, D. Engberg, M. E. Bjorketun, A. Matic, G. Wahnstrom, P. G. Sundell, P. Berastegui, I. Ahmed, P. Falus, B. Farago, L. Borjesson and S. Eriksson, *Chem. Mater.*, 2010, **22**, 740.
- 15 S. B. C. Duval, P. Holtappels, U. Stimming and T. Graule, *Solid State Ionics*, 2008, **179**, 1112.
- 16 N. Ito, H. Matsumoto, Y. Kawasaki, S. Okada and T. Ishihara, *Solid State Ionics*, 2008, **179**, 324.
- 17 M. Karlsson, A. Matic, C. S. Knee, I. Ahmed, S.-G. Eriksson and L. Borjesson, *Chem. Mater.*, 2008, **20**, 3480.
- 18 I. Antunes, A. Brandao, F. M. Figueiredo, J. R. Frade, J. Gracio and D. P. Fagg, *J. Solid State Chem.*, 2009, **182**, 2149.
- 19 M. Karlsson, A. Matic, D. Engberg, M. E. Bjorketun, M. M. Koza, I. Ahmed, G. Wahnstrom, L. Borjesson and S.-G. Eriksson, *Solid State Ionics*, 2009, **180**, 22.
- 20 F. Giannici, A. Longo, A. Balerna, K. D. Kreuer and A. Martorana, *Chem. Mater.*, 2009, **21**, 2641.
- 21 P. Babilo, T. Uda and S. M. Haile, *J. Mater. Res.*, 2007, **22**, 1322.
- 22 P. Babilo and S. M. Haile, *J. Am. Ceram. Soc.*, 2005, **88**, 2362.
- 23 Y. Yamazaki, P. Babilo and S. M. Haile, *Chem. Mater.*, 2008, **20**, 6352.
- 24 Y. Yamazaki, R. Hernandez-Sanchez and S. M. Haile, *Chem. Mater.*, 2009, **21**, 2755.
- 25 J. H. Shim, J. S. Park, J. An, T. M. Gur, S. Kang and F. B. Prinz, *Chem. Mater.*, 2009, **21**, 3290.
- 26 S. Zhang, L. Bi, L. Zhang, Z. Tao, W. Sun, H. Wang and W. Liu, *J. Power Sources*, 2009, **188**, 343.
- 27 J. R. Tolchard and T. Grande, *Solid State Ionics*, 2007, **178**, 593.
- 28 S. Tao and J. T. S. Irvine, *J. Solid State Chem.*, 2007, **180**, 3493.
- 29 A. K. Azad, C. Savaniu, S. Tao, S. Duval, P. Holtappels, R. M. Ibberson and J. T. S. Irvine, *J. Mater. Chem.*, 2008, **18**, 3414.
- 30 A. S. Patnaik and A. V. Virkar, *J. Electrochem. Soc.*, 2006, **153**, A1397–A1405.
- 31 K. D. Kreuer, *Solid State Ionics*, 1999, **125**, 285.
- 32 W. Munch, G. Seifert, K. D. Kreuer and J. Maier, *Solid State Ionics*, 1997, **97**, 39.
- 33 M. E. Bjorketun, P. G. Sundell and G. Wahnstrom, *Phys. Rev. B*, 2007, **76**, 054307.
- 34 B. Merinov and W. A. Goddard, *J. Chem. Phys.*, 2009, **130**, 194707.
- 35 M. E. Bjorketun, P. G. Sundell and G. Wahnstrom, *Faraday Discuss.*, 2007, **134**, 247.
- 36 P. G. Sundell, M. E. Bjorketun and G. Wahnstrom, *Phys. Rev. B*, 2007, **76**, 094301.
- 37 P. G. Sundell, M. E. Bjorketun and G. Wahnstrom, *Phys. Rev. B*, 2006, **73**, 104112.
- 38 Q. Zhang, G. Wahnstrom, M. E. Bjorketun, S. Gao and E. Wang, *Phys. Rev. Lett.*, 2008, **101**, 215902.
- 39 M. S. Islam, P. R. Slater, J. R. Tolchard and T. Dinges, *Dalton Trans.*, 2004, 3061.
- 40 K. A. Furoy, R. Haugrud, M. Hansel, A. Magraso and T. Norby, *Solid State Ionics*, 2007, **178**, 461.
- 41 C. Y. Jones, J. Wu, L. P. Li and S. M. Haile, *J. Appl. Phys.*, 2005, **97**, 114908.
- 42 T. Fukui, S. Ohara and S. Kawatsu, *J. Power Sources*, 1998, **71**, 164.
- 43 C. S. Knee, A. Magraso, T. Norby and R. I. Smith, *J. Mater. Chem.*, 2009, **19**, 3238.
- 44 A. Magraso, A. Calleja, X. G. Capdevila and F. Espiell, *Solid State Ionics*, 2004, **166**, 359.
- 45 A. Magraso, F. Espiell, M. Segarra and J. T. S. Irvine, *J. Power Sources*, 2007, **169**, 53.
- 46 S. Mimuro, S. Shibako, Y. Oyama, K. Kobayashi, T. Higuchi, S. Shin and S. Yamaguchi, *Solid State Ionics*, 2007, **178**, 641.
- 47 A. Magraso, R. Haugrud, M. Segarra and T. Norby, *J. Electroceram.*, 2009, **23**, 80.
- 48 P. J. Saines, B. J. Kennedy and R. I. Smith, *Mater. Res. Bull.*, 2009, **44**, 874.
- 49 R. A. Davies, M. S. Islam and J. D. Gale, *Solid State Ionics*, 1999, **126**, 323.
- 50 M. S. Islam, R. A. Davies, C. A. J. Fisher and A. V. Chadwick, *Solid State Ionics*, 2001, **145**, 333.
- 51 J. Wu, R. A. Davies, M. S. Islam and S. M. Haile, *Chem. Mater.*, 2005, **17**, 846.
- 52 G. C. Mather and M. S. Islam, *Chem. Mater.*, 2005, **17**, 1736.
- 53 M. S. Islam, *J. Mater. Chem.*, 2000, **10**, 1027.
- 54 E. Kendrick, J. Kendrick, K. S. Knight, M. S. Islam and P. R. Slater, *Nat. Mater.*, 2007, **6**, 871.
- 55 M. S. Islam and P. R. Slater, *MRS Bull.*, 2009, **34**, 935.
- 56 C. R. A. Catlow, *Solid State Chemistry: Techniques*, Clarendon Press, Oxford.
- 57 B. G. Dick and A. W. Overhauser, *Phys. Rev.*, 1958, **112**, 90.
- 58 N. F. Mott and M. J. Littleton, *J. Chem. Soc., Faraday Trans. 2*, 1989, **85**, 565.
- 59 J. D. Gale, *J. Chem. Soc., Faraday Trans.*, 1997, **93**, 629.
- 60 G. V. Lewis and C. R. A. Catlow, *J. Phys. C*, 1985, **18**, 1149.
- 61 M. S. Khan, M. S. Islam and D. R. Bates, *J. Mater. Chem.*, 1998, **8**, 2299.
- 62 P. Saul and C. R. A. Catlow, *Philos. Mag. B*, 1985, **51**, 107.
- 63 K. P. Schroder, J. Sauer, M. Leslie, C. R. A. Catlow and J. M. Thomas, *Chem. Phys. Lett.*, 1992, **188**, 320.
- 64 R. Glockner, M. S. Islam and T. Norby, *Solid State Ionics*, 1999, **122**, 145.
- 65 P. Panchmatia, A. Orera, J. Hanna, M. E. Smith, P. R. Slater and M. S. Islam, *J. Mater. Chem.*, 2010, **20**, 2766.
- 66 Y. Hinatsu, *J. Solid State Chem.*, 1996, **122**, 384.
- 67 A. J. Jacobson, B. Tofield and B. E. F. Fender, *Acta Crystallogr., Sect. B: Struct. Crystallogr. Cryst. Chem.*, 1972, **B28**, 956.
- 68 W. Munch, K. D. Kreuer, G. Seifert and J. Maier, *Solid State Ionics*, 2000, **136**, 183.
- 69 M. S. Islam, R. A. Davies and J. D. Gale, *Chem. Mater.*, 2001, **13**, 2049.
- 70 K. Wright, R. Freer and C. R. A. Catlow, *Phys. Chem. Miner.*, 1995, **20**, 500.
- 71 C. R. A. Catlow, *J. Phys. Chem. Solids*, 1977, **38**, 1131.
- 72 C. Karmonik, T. J. Udovic, R. L. Paul, J. J. Rush, K. Lind and R. Hempelmann, *Solid State Ionics*, 1998, **109**, 207.
- 73 R. Hempelmann, M. Soetratmo, O. Hartmann and R. Wappling, *Solid State Ionics*, 1998, **107**, 269.
- 74 W. G. Coors, *J. Power Sources*, 2003, **118**, 150.
- 75 M. Yashima, K. Nomura, H. Kageyama, Y. Miyazaki, N. Chitose and K. Adachi, *Chem. Phys. Lett.*, 2003, **380**, 391.
- 76 M. Yashima, *Solid State Ionics*, 2008, **179**, 797.